Calorimetric Analysis of Triple Helices Targeted to the d($G_3A_4G_3$)·d($C_3T_4C_3$) Duplex†

P. V. Scaria and Richard H. Shafer*

Department of Pharmaceutical Chemistry, School of Pharmacy, University of California, San Francisco, California 94143

Received April 22, 1996; Revised Manuscript Received June 18, 1996⊗

ABSTRACT: We present a thermodynamic analysis based on differential scanning calorimetry (DSC) of three short intermolecular DNA triplexes targeted to the same DNA duplex: d($C^+_3T_4C^+_3$)*d-($G_3A_4G_3$)·d($C_3T_4C_3$) (PYR), d($G_3A_4G_3$)*d($G_3A_4G_3$)·d($C_3T_4C_3$) (PUR), and d($G_3T_4G_3$)*d($G_3A_4G_3$)·d($C_3T_4C_3$) (PUR/PYR). Enthalpies, ΔH, and entropies, ΔS, are measured by model-free integration of the DSC curves and are compared to the same quantities determined by van't Hoff analysis of the DSC curves and, in the case of the PYR and PUR/PYR triplexes, UV melting curves as well. In the case of the PUR triplex, which exhibits monophasic melting behavior, the calorimetric ΔH and the calorimetrically determined van't Hoff ΔH are in excellent agreement, indicating an all-or-none transition for this triplex. For the PYR and PUR/PYR triplexes, which melt in a biphasic manner, the calorimetrically determined van't Hoff ΔH values are somewhat larger than the model-independent calorimetric ΔH values. In those cases, however, good agreement is found between the calorimetric ΔH values and the spectrophotometrically determined van't Hoff ΔH values. The calorimetrically determined ΔH values, expressed per mole of triplet, for the three triplexes are 4.5, 3.8, and 2.4 kcal/mol for the PUR, PYR, and PUR/PYR triplexes, respectively. The same order of stability is observed in terms of ΔG and T_m values. The high stability of the PUR triplex at neutral pH indicates that purine oligonucleotides may be the most effective at targeting duplex regions for triple helix formation *in vivo*.

The triple helix is one of the several unusual nucleic acid structures that have recently become of great interest in terms of both conformational polymorphism and practical applications. These structures are not only interesting in themselves but also in terms of the equilibria governing the transitions between various forms and the effect of environmental factors on such transitions. The potential biological significance of these unusual nucleic acid forms is of paramount importance. Applications of triple helix-forming oligonucleotides include sequence-specific cleavage of chromosomal DNA (Strobel & Dervan, 1992; Strobel et al., 1991), specific inhibition of gene expression as a means of elucidating functional roles of gene products, and antigene activity in the context of therapeutic uses of DNA (Sun & Helene, 1993; Thuong & Helene, 1993). This latter utilization shows promise in the area of antiviral and anticancer chemotherapy (Ebbinghaus et al., 1993). Thus, there is ample impetus for fundamental studies on the structure and stability of triplexes with the aim of elucidating the principles of optimal design of oligonucleotides destined to form triple helices *in vivo*.

Triplex formation requires a homopurine·homopyrimidine motif in the duplex target. There are three major classes of nucleic acid triplexes: those whose third strand is composed primarily of pyrimidines (pyr*pur·pyr triplexes), purines (pur*pur·pyr triplexes), or a mixture of thymine and guanine bases (pyr/pur*pur·pyr triplexes). Here, · represents the Watson−Crick interactions that stabilize the duplex structure while * represents the Hoogsteen-like hydrogen-bonding interaction between the duplex and the third strand. Interestingly, most of the thermodynamic studies have centered on pyr*pur·pyr triplexes [see Singleton and Dervan (1994) and references therein], while most of the studies exploring the biological activity of triplex-forming oligonucleotides *in vivo* have involved pur*pur·pyr or pyr/pur*pur·pyr triplexes (Hobbs & Yoon, 1994; McShan et al., 1992; Postel et al., 1991; Roy, 1994; Scaggiante et al., 1994). More recently, thermodynamic stability measurements have been reported for a pur*pur·pyr triplex, including effects of mismatches at one site (Greenberg & Dervan, 1995).

The diversity with regard to third-strand composition translates into a certain degree of degeneracy in the triplet binding code. For example, either a thymine or an adenine can hydrogen bond to an adenine in the underlying duplex, while a similar choice is possible for either cytosine or guanine with respect to hydrogen bonding to a duplex guanine. Furthermore, both guanine and thymine appear to form Hoogsteen hydrogen bonds in either parallel or antiparallel orientations; adenine is limited to the antiparallel orientation, and cytosine appears to be limited to the parallel orientation (Sun & Helene, 1993).

Thermodynamic analysis provides one approach to understanding the stability of triplexes and its relation to nucleic acid sequence. A variety of reports devoted to thermodynamic analysis of triple helices based on spectrophotometric and calorimetric techniques has appeared (Escude et al., 1993; Manzini et al., 1990; Mergny et al., 1991; Park & Breslauer, 1991; Pilch et al., 1990, 1991; Plum et al., 1990; Scaria et al., 1995; Sun et al., 1991; Volker et al., 1993; Wilson et al., 1994; Xodo et al., 1990, 1991). There are several important issues, addressed in these studies, that need to be considered in the thermodynamic analysis of triplexes in general. One is the question of reversibility of the triplex → duplex + single strand transition, which is required in

† Supported by NSF Grant MCB 9218687.
⊗ Abstract published in *Advance ACS Abstracts,* August 1, 1996.

S0006-2960(96)00966-X CCC: $12.00

the analysis of UV melting curves, perhaps the most common experimental approach to measuring stability of nucleic acid structures. Under certain conditions, it has been shown that the dissociation of the triple helix third strand does not occur reversibly (Rougee et al., 1992). Second is the question of whether this transition is accurately described by the two-state, or all-or-none, model. This latter also underlies the analysis of spectrophotometrically determined melting profiles. Third, in the case of pyr∗pur·pyr triplexes containing protonated cytosines, the effect of protonation, which is coupled to triplex formation, must be considered in the thermodynamic analysis (Manzini et al., 1990; Wilson et al., 1994).

Several additional methods for determining the thermodynamics of triple helix formation have been described. Dervan and co-workers (Best & Dervan, 1995; Greenberg & Dervan, 1995; Singleton & Dervan, 1992a,b, 1993, 1994) have developed a quantitative affinity cleavage method, modeled on DNase I footprinting methods, for studying protein−DNA interactions (Brenowitz et al., 1986). Shindo and co-workers (Shindo et al., 1993) have similarly adapted the filter binding assay for protein−DNA interactions to the analysis of the equilibrium and kinetic properties of triplex formation. Finally, a recent report has appeared on the application of fluorescence resonance energy transfer to triplex thermodynamics (Yang et al., 1994). These methods differ from calorimetric heat determinations in that they involve direct measurement of the binding constant, K, and corresponding $\Delta G°$, with the remaining thermodynamic properties determined from the temperature dependence of K.

There are several reports in the current literature of an unusual discrepancy between enthalpy values measured by direct integration of excess heat capacity curves, ΔH_{CAL}, and those determined by van't Hoff analysis, ΔH_{VH}, for the dissociation of the triple helix third strand (Plum & Breslauer, 1995; Plum et al., 1990; Volker et al., 1993). Comparison of these two measurements is typically used to assess the validity of the all-or-none approximation. This approximation is considered valid when the two enthalpy values are the same, while a larger value of ΔH_{CAL} indicates that intermediate states are involved in the transition. However, in these cases, not only were the two enthalpy values different, but also ΔH_{CAL} was substantially less than ΔH_{VH}. This unusual behavior has been discussed in a recent review by Breslauer and co-workers (Plum et al., 1995b). In this work, we present results of differential scanning calorimetry (DSC)[1] analysis of three different oligonucleotide triplexes based on a common target duplex. Our results for ΔH and ΔS show very good agreement, in general, between values determined by direct integration of the excess heat capacity curves and those determined by van't Hoff analysis of UV melting data, while van't Hoff analysis of the calorimetric data yields, in some cases, larger enthalpy changes than direct integration. These results are discussed in detail below.

MATERIALS AND METHODS

Oligonucleotides. Oligonucleotides were purchased from Genset Corp. or Integrated DNA Technologies, Inc., and were dialyzed extensively against 1 mM Tris using 1000 molecular weight cutoff dialysis tubing. Oligonucleotide purity was checked by HPLC, NMR, and polyacrylamide gel electrophoresis and found to be ≥95%. The concentration of oligonucleotide solutions was determined using the following extinction coefficients, per mole of base, measured by phosphate analysis (Griswold et al., 1951): d($G_3A_4G_3$), $\epsilon_{255} = 11\ 500\ M^{-1}\ cm^{-1}$; d($C_3T_4C_3$), $\epsilon_{272} = 8300\ M^{-1}\ cm^{-1}$; and d($G_3T_4G_3$), $\epsilon_{256} = 9900\ M^{-1}\ cm^{-1}$. Duplex and triplex samples were prepared in 10 mM sodium cacodylate or 10 mM Tris/HCl buffer containing 50 mM $MgCl_2$. Samples for calorimetric studies were dialyzed extensively against the appropriate buffer over several days before use. The dialysate from the final dialysis was used as a reference in the calorimetric runs. All triplexes were formed by mixing stoichiometric amounts of oligonucleotides and then heating to 90 °C for 5 min, followed by slow cooling to ambient temperature.

Calorimetry. Differential scanning calorimetry experiments (Breslauer et al., 1992) were carried out on a Microcal MC2 differential scanning calorimeter. Sample concentrations varied from 0.08 to 0.2 mM structure (duplex or triplex), and the cell volume was 1.2086 mL. The performance of the instrument was calibrated periodically with an electrical pulse and was also checked by comparing the ΔH values obtained for poly(dA-dT) and the self-complementary duplex d(GCGAATTCGC)$_2$. The resulting values for ΔH were in very good agreement with those published previously for these two systems (Breslauer et al., 1986; Marky et al., 1981). Heat capacity vs temperature curves for various samples were obtained at a heating rate of 1 °C/min while collecting the data points at a rate of 5 Hz. Decreasing the heating rate did not change the calculated thermodynamic parameters significantly. For duplex as well as triplex samples, repeated scans resulted in superimposable melting profiles, indicating the reversibility of these transitions. Reversibility was further investigated by UV experiments involving melting followed by cooling at identical rates.

Data Analysis. Heat capacity vs temperature profiles were calculated by subtracting buffer vs buffer curves from the sample vs buffer curves. The data were then normalized with regard to the concentration and cell volume. The resulting heat capacity curves were analyzed using the manufacturer's software, Origin for DSC. Integration of these curves requires construction of a baseline, which can be problematic if, as in the case of some of the triplexes investigated here, the pre- and post-transition regions of heat capacity curves are not flat. This has been discussed in several recent DSC studies on nucleic acid structures (Gluick & Draper, 1994; Hopkins et al., 1993; Park & Breslauer, 1991). In the procedure we have selected, using the Origin software, the program picks two linear segments on the curve, one before the beginning of the transition, and one after the transition and connects the two segments according to the slope and intercept, rather than the end points, of the selected regions and calculates the baseline in the transition region on the basis of the progress or extent of the reaction. This baseline was the only one that uniformly gave good agreement between ΔH_{CAL} for the duplex samples and the ΔH_{VH} determined by deconvoluting the triplex heat capacity curves. An alternative baseline, determined by a cubic polynomial fit to the pre- and post-transition segments of the heat capacity curves, gave similar results in most cases.

[1] Abbreviations: CD, circular dichroism; DSC, differential scanning calorimetry.

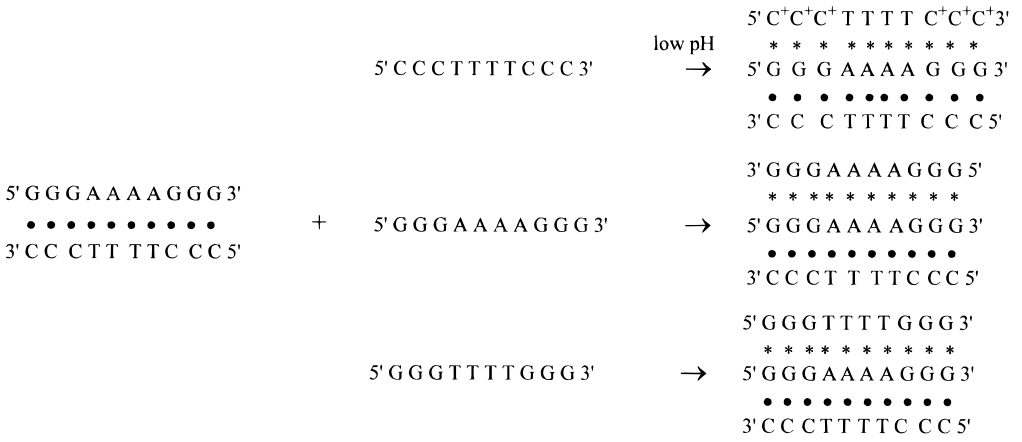

FIGURE 1: Schematic representation of the three triplexes based on the target duplex, $d(G_3A_4G_3)\cdot d(C_3T_4C_3)$.

Calorimetric transition enthalpies, ΔH_{CAL}, were then obtained by integrating the area under the heat capacity vs temperature curves, i.e. $\Delta H_{CAL} = \int C_p dT$. Similarly, values for entropy change, ΔS_{CAL}, accompanying the melting of the duplex and triplex samples, were determined by integrating the curve obtained by dividing the heat capacity curve by the absolute temperature, i.e. $\Delta S_{CAL} = \int (C_p/T) dT$. Free energies were calculated following a recently proposed method (Plum et al., 1995a) that combines ΔH_{CAL} with results from UV analysis in the integrated form of the Gibbs−Helmholtz equation:

$$\Delta G(298) = \Delta H_{CAL}\left(1 - \frac{298}{T_{max}}\right) + 298R \ln\left[n^{(n/2-1)}\left(\frac{\sqrt{n}+1}{C_{tot}}\right)^{(n-1)}\right]$$

where T_{max} is the temperature corresponding to the maximum in the derivative of the absorbance vs temperature curve for a particular value of C_{tot} (the total concentration of interacting species, except for the PUR triplex, where C_{tot} is twice the purine strand concentration) and n is the molecularity of the complex, i.e. the number of species coming together in the complex. Note that the above equation is written for the dissociation process. The reported values for ΔG are averages over pairs of T_{max} and C_{tot} values from UV melting curves.

The calorimetric melting profiles were also modeled by either a single transition or two sequential, all-or-none transitions. For a single transition, the expressions relevant to non-self-complementary duplexes or to the direct dissociation of a triplex to single strands can be programmed as a user-defined fitting funtion in the Origin software and the best fit parameters determined by nonlinear curve fitting. In the case of two sequential bimolecular reactions, the enthalpies can be determined by simulation of the resulting set of coupled, nonlinear equations. This is outlined in detail in the Appendix. The resulting enthalpy changes are denoted $\Delta H_{VH(cal)}$. As mentioned below, we assume enthalpy and entropy changes to be independent of temperature. Corresponding values for entropy changes, $\Delta S_{VH(cal)}$, were calculated at T_m from the equation

$$\Delta S_{VH(cal)} = R \ln K(T_m) + \frac{\Delta H_{VH(cal)}}{T_m}$$

and assumed to be the same at other temperatures.

Finally, we compare these results, based on calorimetry, to our previously published results based on the concentration dependence of melting temperatures, determined from UV absorbance vs temperature curves. The enthalpy and entropy changes thus determined are denoted $\Delta H_{VH(uv)}$ and $\Delta S_{VH(uv)}$, respectively. Changes in all thermodynamic functions are presented for the actual endothermic dissociation processes measured, i.e. all enthalpies and entropies are positive numbers.

RESULTS AND DISCUSSION

The three different classes of triplexes studied here were formed by targeting the duplex $d(G_3A_4G_3)\cdot d(C_3T_4C_3)$ with either $d(G_3A_4G_3)$, $d(C_3T_4C_3)$, or $d(G_3T_4G_3)$ oligonucleotides to give the following triplexes: $d(G_3A_4G_3)*d(G_3A_4G_3)\cdot d(C_3T_4C_3)$ (denoted PUR), $d(C_3T_4C_3)*d(G_3A_4G_3)\cdot d(C_3T_4C_3)$ (PYR), and $d(G_3T_4G_3)*d(G_3A_4G_3)\cdot d(C_3T_4C_3)$ (PUR/PYR), respectively. Figure 1 depicts the schematic representation of the various triplexes studied. The PYR triplex is stabilized at low pH because the cytosines in the third strand need to be protonated in order to form two Hoogsteen hydrogen bonds with the purine bases of the duplex. Hence, all the experiments for this triplex were carried out at pH = 5.3. The other two triplexes do not require low pH for their formation and hence were investigated at pH = 7.5. Sodium cacodylate (10 mM) was used to buffer the PUR and PYR triplex samples. We have shown earlier (Keniry et al., 1995; Scaria et al., 1992; Strahan et al., 1994) that the oligonucleotide $d(G_3T_4G_3)$, used as the third strand in the PUR/PYR triplex, self-associates in the presence of monovalent cations such as Na^+ or K^+ via guanine quartet formation. In order to avoid this self-association, Tris/HCl was used as the buffer in this case. The 50 mM $MgCl_2$ used for stabilizing the triplexes did not induce quadruplex formation in the $d(G_3T_4G_3)$ samples. Similarly, the third strand, $d(C_3T_4C_3)$, in the PYR triplex also has the potential to form self-associated duplex structures stabilized by C^+-C base pairs at low-pH conditions (Pilch & Shafer, 1993). However, following heating and cooling in the presence of stoichiometric amounts of the duplex target, all $d(C_3T_4C_3)$ is complexed to the duplex (Pilch et al., 1990)

In Figure 2, we present UV melting profiles of these triplexes along with cooling profiles, obtained at a heating−cooling rate of 1 °C/min, the same rate used in our DSC measurements. These heating−cooling profiles are almost

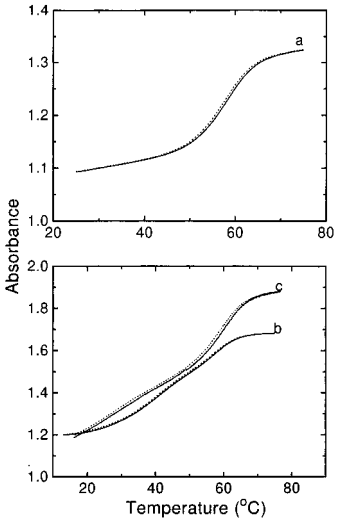

FIGURE 2: Temperature-induced denaturation (solid lines) and renaturation (dashed lines) profiles for various triplexes monitored by UV absorbance changes at 260 nm (a and b) or 275 nm (c). a−c correspond to the triplexes formed by targeting $d(G_3A_4G_3)$·$d(C_3T_4C_3)$ with $d(G_3A_4G_3)$, $d(C_3T_4C_3)$, or $d(G_3T_4G_3)$, respectively, in the presence of 50 mM $MgCl_2$ and 10 mM sodium cacodylate buffer with pH = 7.5 (a) or pH = 5.3 (b) or 10 mM Tris/HCl with pH = 7.5 (c). Heating and cooling rates were 1 °C/min. Concentrations were as follows: a, 0.05 mM triplex; b, 0.05 mM triplex; and c, 0.1 mM triplex (c is offset by 1.5 absorbance units).

superimposable and thus indicate that these transitions occur in a reversible, or quasi-reversible, manner under our experimental conditions. This is important because the determination of ΔS from calorimetric data requires that the observed transitions occur reversibly. Reversibility is also necessary in estimating the model-dependent thermodynamic parameters using van't Hoff analysis of either UV melting data or calorimetry data.

Figure 3 presents the heat capacity vs temperature profiles for the duplex common to all three triplexes, as well as for the triplexes themselves. The heat capacity curve for the duplex, in the absence of the third strand, reaches a maximum at 56 °C (Figure 3A, 0.08 mM duplex), showing the dissociation of the double helix at this temperature and concentration. The PUR triplex also shows a single peak at 62 °C (Figure 3B, 0.18 mM triplex), consistent with the monophasic melting established for this triplex by a variety of techniques (Pilch et al., 1991).

Figure 3C shows the calorimetric melting profile of the PYR triplex at pH = 5.3. As observed in the UV melting profiles, the heat capacity vs temperature curve is biphasic, with the low-temperature transition centered around 45 °C (0.1 mM triplex) due to the dissociation of the third strand from the target duplex and the high-temperature transition at 60 °C due to dissociation of the duplex strands. In the UV melting studies, the two transitions were well-separated, whereas these transitions are much closer in the calorimetry experiments. This is due to a larger concentration dependence of the triplex dissociation compared to the duplex dissociation, arising from the smaller enthalpy change for triplex dissociation. A qualitatively similar melting behavior is observed for the PUR/PYR triplex at neutral pH solutions, although the resolution of the two transitions is better due to the lower third-strand dissociation temperature (Figure 3D). In both cases of multiple transitions, the pretransition baseline region is limited.

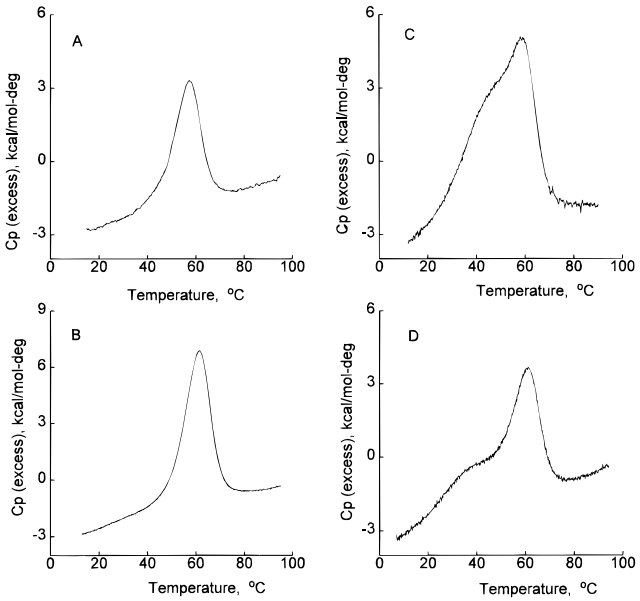

FIGURE 3: Excess heat capacity vs temperature curves obtained for the $d(G_3A_4G_3)$·$d(C_3T_4C_3)$ duplex (A) and triplexes formed by targeting the duplex with $d(G_3A_4G_3)$ (B), $d(C_3T_4C_3)$ (C), or $d(G_3T_4G_3)$ (D) in the presence of 50 mM $MgCl_2$ and 10 mM sodium cacodylate buffer with pH = 7.5 (A and B) or pH = 5.3 (C) or 10 mM Tris/HCl with pH = 7.5 (D). The curves represent the heat capacity vs temperature data obtained by subtracting the buffer vs buffer scans from sample vs buffer scans, followed by normalization with respect to concentration and cell volume. Concentrations were as follows: A, 0.08 mM duplex; B, 0.18 mM triplex; C, 0.1 mM triplex; and D, 0.2 mM triplex. The heating rate was: 1 °C/min.

Table 1: Thermodynamic Parameters for the $d(G_3A_4G_3)$·$d(C_3T_4C_3)$ Duplex[a]

	$d(G_3A_4G_3)$·$d(C_3T_4C_3)$	
	pH 7.5	pH 5.3
$\Delta H°$ (kcal/mol)		
$\Delta H°_{CAL}$	71 ± 1	72 ± 2
$\Delta H°_{VH(cal)}$	77 ± 1	73 ± 1
$\Delta H°_{VH(uv)}$	72 ± 9[b]	77 ± 10[c]
$\Delta S°$ (cal/mol-deg)		
$\Delta S°_{CAL}$	216 ± 2	218 ± 6
$\Delta S°_{VH(cal)}$	215 ± 2	201 ± 4
$\Delta S°_{VH(uv)}$	198 ± 30[b]	215 ± 31[c]
ΔG (kcal/mol)		
$\Delta G°$	12.6 ± 0.1	12.8 ± 0.1
$\Delta G°_{VH(uv)}$	12.6 ± 0.7[b]	13.1 ± 0.8[c]
T_m (°C), from van't Hoff analysis	56.0 ± 0.1[d]	57 ± 0.2[e]

[a] Errors in calorimetric values represent the standard deviation of results on five or six calorimetric scans of the same sample, while errors in the van't Hoff analysis of calorimetric data represent the standard deviations of values obtained from analysis of the same five or six scans. Errors in ΔG° represent the standard deviation of values using the the range of ΔH_{CAL} values. [b] From Pilch et al. (1991). [c] Pilch (1991). [d] 0.08 mM duplex/ [e] 0.16 mM duplex.

Calorimetric Enthalpy Changes. The model-independent analysis of these calorimetric data by direct integration of the heat capacity curves is summarized in Tables 1 and 2, in terms of the enthalpy and entropy changes accompanying the various transitions. The ΔH_{CAL} for the $d(G_3A_4G_3)$·$d(C_3T_4C_3)$ duplex at neutral pH is 71 ± 1 kcal/mol which is close to the van't Hoff enthalpy change we reported earlier, on the basis of the analysis of the concentration dependence of the melting temperature (Pilch et al., 1991). Interestingly, these values are significantly less than what is predicted (84.7 kcal/mol) on the basis of nearest neighbor calculations

Table 2: Thermodynamic Parameters for Triplexes Targeted to $d(G_3A_4G_3)\cdot d(C_3T_4C_3)$[a]

triplex third strand	$d(G_3T_4G_3)$	$d(G_3A_4G_3)$	$d(C_3T_4C_3)$
$\Delta H°$(total) (kcal/mol)			
$\Delta H°_{CAL}$	95 ± 3	116 ± 1	110 ± 2
$\Delta H°_{VH(cal)}$	112 ± 2	115 ± 1	121 ± 3
$\Delta H°_{VH(uv)}$	86 ± 6[b]		114 ± 6[c]
$\Delta H°(1)$ (kcal/mol)			
$\Delta H°_{CAL}$	24 ± 7	45 ± 2	38 ± 4
$\Delta H°_{VH(cal)}$	33 ± 1		51 ± 2
$\Delta H°_{VH(uv)}$	20 ± 2[b]		42 ± 4.1[c]
$\Delta H°(2)$ (kcal/mol)			
$\Delta H°_{CAL}$ (from Table 1)	71 ± 1	71 ± 1	72 ± 2
$\Delta H°_{VH(cal)}$	79 ± 1		70 ± 1
$\Delta H°_{VH(uv)}$	66 ± 4[b]		72.9 ± 1.9[c]
$\Delta S°$(total) (cal mol^{-1} K^{-1})			
$\Delta S°_{CAL}$	289 ± 9	350 ± 4	337 ± 7
$\Delta S°_{VH(cal)}$	307 ± 5	309 ± 1	336 ± 7
$\Delta S°_{VH(uv)}$	226 ± 20[b]		322 ± 20[c]
$\Delta S°(1)$ (cal mol^{-1} K^{-1})			
$\Delta S°_{CAL}$	73 ± 11	134 ± 6	119 ± 18
$\Delta S°_{VH(cal)}$	89 ± 3		143 ± 4
$\Delta S°_{VH(uv)}$	47 ± 5[b]		120 ± 14[c]
$\Delta S°(2)$ (cal mol^{-1} K^{-1})			
$\Delta S°_{CAL}$ (from Table 1)	216 ± 2	216 ± 2	218 ± 6
$\Delta S°_{VH(cal)}$	218 ± 2		193 ± 3
$\Delta S°_{VH(uv)}$	179 ± 15[b]		202 ± 6[c]
$T_m(1)$ (°C), from van't Hoff analysis	36 ± 1[d]	60.0 ± 0.1[e] (single transition)	44.4 ± 0.4[f]
$T_m(2)$ (°C), from van't Hoff analysis	62 ± 0.1[d]		56.5 ± 0.1[f]

[a] **1** and **2** denote the first (low-temperature) and second (high-temperature) transitions, respectively, and total denotes the sum for the two transitions. Errors in calorimetric values represent the standard deviation of values from six to nine repeat scans on the same sample, while errors in the van't Hoff analysis of calorimetric data represent the standard deviation of values (determined by simulation or curve fitting) from analysis of the same six to nine scans. [b] From Scaria et al. (1995) and unpublished data. [c] Pilch et al. (1990). [d] $T_m(1)$ and $T_m(2)$ defined such that $K_1T_m(1) = C_t/2$ and $K_2T_m(2) = C_t/2$, where C_t is the initial, triplex concentration; data obtained at 0.2 mM triplex [e] T_m defined as the midpoint of the transition triplex → single strands; data obtained at 0.18 mM triplex. [f] T_m values defined as in footnote *d*; data obtained at 0.1 mM triplex.

(Breslauer et al., 1986). This discrepancy may be due to the differences in the solution conditions and, more significantly, due to the presence of blocks of guanines in the sequence, which have been reported to yield unusually low values of ΔH (Breslauer et al., 1986). The values of ΔH_{CAL} for the duplex at two different pH values (pH = 7.5 and 5.3) are fairly similar, as are the T_m values, indicating the absence of any major effect of pH on the duplex thermodynamics in this pH range.

The ΔH_{CAL} values corresponding to the dissociation of the third strand from the triplex were obtained by subtracting the ΔH_{CAL} for the duplex determined independently under appropriate solution conditions from the total enthalpy change for dissociation of the triplexes to single strands. This procedure assumes that the presence of the dissociated third strand does not contribute to the observed signal, i.e. that there is no structure in the dissociated strand which itself melts as the temperature continues to increase. This assumption seems reasonable, since the deconvolution of the triplex calorimetry curves gives similar ΔH values for the dissociation of the underlying duplex compared to that of the free duplex (see below). Also, UV melting studies showed no sign of significant structure in the third strand alone at temperatures exceeding that corresponding to dissociation of the third strand of these triplexes. The value

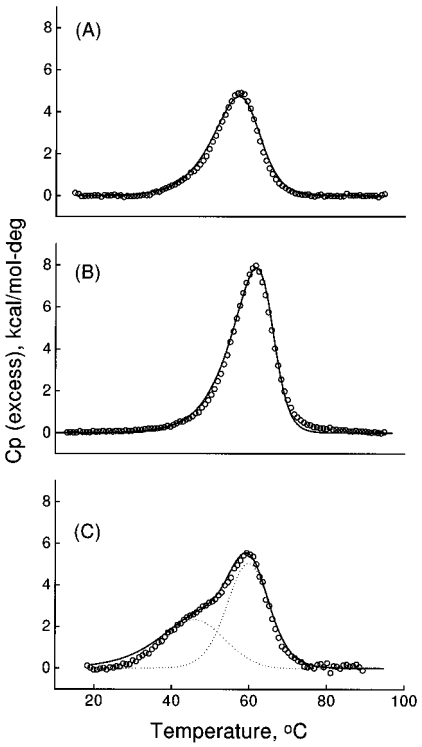

FIGURE 4: Excess heat capacity vs temperature curves obtained for the $d(G_3A_4G_3)\cdot d(C_3T_4C_3)$ duplex (A) and triplexes formed by targeting the duplex with $d(G_3A_4G_3)$ (B) or $d(C_3T_4C_3)$ (C) (see Figure 3 for experimental conditions): (○) experimental data after baseline subtraction; (—) theoretical curve obtained by nonlinear curve fitting (A) or simulation (B) and (C), according to a model consisting of a single two-state transition (A and B) or two sequential, two-state transitions (C); and (···) deconvoluted curves representing the two transitions in part C corresponding to the third strand dissociation and the duplex dissociation, respectively.

of ΔH_{CAL} for third-strand dissociation is highest for the PUR triplex (45 kcal/mol). Dissociation of the third strand from the PYR triplex is accompanied by an enthalpy change of 38 kcal/mol, while dissociation of the PUR/PYR triplex entails only 24 kcal/mol.

Comparison with van't Hoff Enthalpies. The van't Hoff enthalpy values, $\Delta H_{VH(cal)}$, obtained from either simulation (PYR and PUR/PYR triplexes, two transitions) or nonlinear regression analysis (duplex and PUR triplex, one transition) of the heat capacity vs temperature curves, are included in Tables 1 and 2, and the corresponding deconvolutions of the heat capacity curves are presented in Figures 4 and 5. In the case of the duplex and the PUR triplex, where ample low-temperature baseline data could be obtained, no significant ΔC_p was observed. But for the other two triplexes, due to the lack of a sufficient low-temperature baseline, the sloping nature of the baselines, and the observed overlap of transitions, this could not be determined with a high degree of certainty. Previous calorimetric studies on triplexes with pyrimidine third strands have found no ΔC_p associated with the triplex transition (Hopkins et al., 1993; Plum & Breslauer, 1995; Plum et al., 1990; Singleton & Dervan, 1994; Xodo et al., 1990). Although there is one report of a possible ΔC_p for one such triplex, determined by filter binding studies (Shindo et al., 1993), this was explained as most likely arising from self-structure in the pyrimidine strand at low pH. Hence, it seems reasonable to assume that $\Delta C_p = 0$ in modeling all of the heat capacity curves.

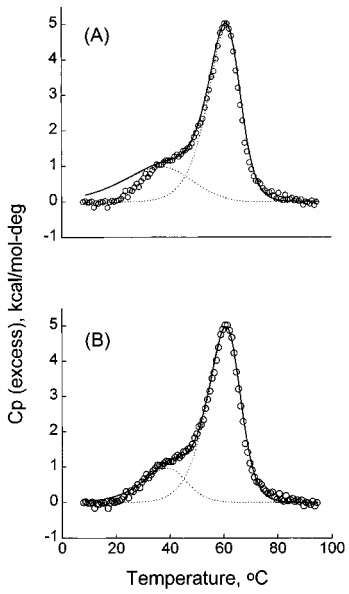

FIGURE 5: Heat capacity vs temperature curves for the PUR/PYR triplex, d($G_3T_4G_3$)*d($G_3A_4G_3$)·d($C_3T_4C_3$): (○) experimental data after baseline subtraction, (—) total simulated transition, and (•••) deconvolution into subtransitions. (A) Simple simulation and (B) more extended simulation (see the Appendix for details).

The duplex curves are modeled closely by a single two-state transition, as indicated in Figure 4A, and the resulting $\Delta H_{VH(cal)}$ values at both pH = 7.5 and 5.3 are in good agreement with the model-free ΔH_{CAL} values (see Table 1). In the case of the PUR triplex, the best fit, based on simulation of two sequential transitions, led to convergence of the two T_m values, and collapse of the two subtransitions to a single transition, confirming our previous results (Pilch et al., 1991). The data were then analyzed by nonlinear curve fitting for the direct dissociation of the triplex to single strands. These data were also examined by simulation of the same, one-transition process, and the resulting $\Delta H_{VH(cal)}$ and T_m values were indistinguishable from those obtained by nonlinear curve fitting. This agreement between simulation and curve fitting provides confidence in the results obtained by simulation. From Table 2, it can be seen that the $\Delta H_{VH(cal)}$ (115 kcal/mol triplex) for the single transition is almost identical to the total, integrated ΔH_{CAL} (116 kcal/mol triplex). The excellent agreement between the $\Delta H_{VH(cal)}$ and ΔH_{CAL} values for dissociation of the PUR triplex indicates that this triplex dissociates in an all-or-none fashion.

The $\Delta H_{VH(cal)}$ values for the PYR and PUR/PYR triplexes were obtained by simulation of the data with two sequential all-or-none transitions, and the results are summarized in Figure 4C and 5 and Table 2. The agreement between the total $\Delta H_{VH(cal)}$ (triplex → duplex → single strands) and the total integrated values of the enthalpy changes is reasonable for both triplexes, as is the agreement between the two values for the second transition in both of these triplexes.

The discrepancy between the ΔH_{CAL} and $\Delta H_{VH(cal)}$ for the low-temperature transition in the PYR and PUR/PYR triplexes is significant, with $\Delta H_{VH(cal)}$ about 35% larger than ΔH_{CAL} in each case. Examination of the simulated and experimental heat capacity curves reveals that these differences arise mainly from the fit at the early stages of the first transition, where the simulated curves lie above the experimental curves, the fit being substantially worse in the case of the PUR/PYR triplex. There are several possible sources of these discrepancies. One involves the difficulty in obtaining good experimental low-temperature baselines for these two triplexes. A second possibility that explains the larger van't Hoff enthalpies in comparison to the calorimetric enthalpies is triplex aggregation. While we have not observed evidence for this from spectrophotometric studies on these triplexes, the calorimetry data may be more sensitive to aggregation.

In order to examine these results in greater detail, we implemented a more general analysis of the PUR/PYR data by simulating the heat capacity curves with the calorimetric and van't Hoff enthalpy terms represented as independent parameters, rather than assuming they are equal (see the Appendix). In the case of the PYR triplex, the resulting fit and parameters were marginally different from the simpler simulation, suggesting that baseline determination is likely the major source of discrepancy between experimental and simulated data. Furthermore, the higher melting temperature and the presence of protonated cytosines is expected to minimize the possibility of aggregation. In the case of the PUR/PYR triplex, however, this type of aggregation is more likely and the discrepancy between the experimental and simulated data is significantly greater than for the PYR triplex. This more extended simulation resulted in a substantially improved fit to the experimental curves (see Figure 5), with $\Delta H_{VH(cal)} = 52 \pm 1$ kcal/mol and the simulated calorimetric enthalpy change, $\Delta H_{CAL(sim)}$, $= 21 \pm 2$ kcal/mol. These results are consistent with aggregation at low temperatures for this triplex resulting in a cooperative unit greater than a single triplex.

Tables 1 and 2 also provide $\Delta H_{VH(uv)}$ values reported for these transitions, derived from analysis of the concentration dependence of the melting temperature measured spectrophotometrically under identical solution conditions. These values are in very good agreement for the duplex, for the two transitions of the PYR triplex, and also for the second transition of the PUR/PYR triplex. However, $\Delta H_{VH(uv)}$ for the first transition of the PUR/PYR triplex is 20% smaller than the calorimetric value. Due to the relatively large uncertainty in ΔH_{CAL}, however, this difference may not be significant.

Calorimetric Entropy Changes. The entropic changes associated with the duplex and triplex formation, ΔS_{CAL}, obtained by integrating the area under the C_p/T vs temperature curves, are also tabulated in Table 1. In each case, the ΔS_{CAL} for the dissociation of the third strand from target duplex was obtained by subtracting ΔS_{CAL} for the duplex dissociation from the total integrated value for the triplex. In comparing entropy changes for different triplexes, we must take into account the fact that changes in entropy are heavily dependent on solution conditions, such as the presence of counterions, the amount of bound water molecules, hydrophobic interactions, etc. (Plum et al., 1995b). While we have tried to minimize differences in solution conditions, each sample is somewhat different. Thus, the PYR triplex required an acidic pH, while the PUR/PYR triplex was studied in Tris-containing buffer in order to prevent quadruplex formation in the d($G_3T_4G_3$) third strand.

Changes in entropy, ΔS_{CAL}, for the duplex are presented in Table 1, while those for the triplexes are given in Table 2. Dissociation of the third strand from the PUR triplex yields the largest entropy change, consistent with a very tight interaction with the duplex. The ΔS_{CAL} value for dissociation

of the third strand from the PUR/PYR is the lowest of all three triplexes. Several explanations for the small entropy change are conceivable. One factor may lie in some degree of structural order remaining upon dissociation of the third strand. We might expect this effect to be more pronounced in the case of a triplex whose third strand is released at lower temperatures. Another possibility is the disorder in the triplex attributable to the presence of the nonisomorphous G∗G·C and T∗A·T triplets. As mentioned above, this sample was analyzed in a different buffer system than the other triplexes. However, values of ΔS_{CAL} for dissociation of the target duplex under different buffer conditions are very similar, suggesting that buffer conditions are not the major source of differences observed between ΔS_{CAL} for dissociation of the PUR/PYR triplex and that for the other triplexes.

Comparison with van't Hoff Entropies. As in the case of the enthalpies, the values of $\Delta S_{VH(cal)}$ for the total dissociation of the triplexes are in good agreement with those determined calorimetrically, the largest difference being 12% for the PUR triplex. Again, when broken down to separate terms for triplex and duplex dissociation, the variation is a little greater, although no clear trend is apparent with regard to relative magnitudes. The agreement between ΔS_{CAL} and $\Delta S_{VH(uv)}$ for dissociation of the third strand is very good in the case of the PYR triplex but considerably poorer for the PUR/PYR triplex. In the latter, the result for $\Delta S_{VH(uv)}$ appears anomalously low, compared to values of $\Delta S_{VH(uv)}$ for other triplexes as well as values of $\Delta S_{VH(cal)}$ for this PUR/PYR triplex. One possible explanation may lie in the necessity for measuring UV melting curves at relatively high concentrations, some higher than those used in the calorimetry experiments, due to the inherently low stability of the PUR/PYR triplex (Scaria et al., 1995) and the need to cover a substantial concentration range. This may have enhanced the influence of possible residual structure in the third strand after dissociation. It is also possible that such structure could have a larger impact on the entropy change than on the enthalpy change. Furthermore, due to the broad nature of the transition corresponding to dissociation of the third strand from this triplex, the spectrophotometrically measured T_m values at the lower oligonucleotide concentrations are subject to relatively high uncertainty. Thus, the calorimetrically determined data are probably more reliable than those determined spectrophotometrically.

Free Energy Changes. We have followed the approach of Plum et al. (1995a) in determining free energy changes. This combination of calorimetrically measured enthalpy changes with UV melting results provides a means of determining ΔG with much better relative uncertainties than using the relationship $\Delta G = \Delta H - T\Delta S$, particularly when small values of ΔG arise from the difference of two numbers with a similar magnitude and sign. Examination of Tables 1 and 3 reveals excellent agreement for all triplexes studied between these free energy changes and those determined solely by analysis of UV melting curves. This is perhaps not surprising as both sets of results rely to some extent on the UV data.

Comparison with Other Results. Most of the reported thermodynamic studies on triple helices have been carried out on triplexes with all-pyrimidine third strands. Values for ΔH_{CAL} range from 2 to 7.7 kcal/mol of triplet (Manzini et al., 1990; Plum & Breslauer, 1995; Plum et al., 1990; Volker et al., 1993; Xodo et al., 1990). This range of results is due to a variety of factors, such as base composition and sequence, solution conditions, such as $MgCl_2$ concentration and/or pH. Our result of 3.8 kcal per mole of base triplet is in good accord with those values. As in the other cases cited, results for the PYR triplex include the contribution due to protonation of the cytosine residues. At pH = 5.3, about one-third of the cytosine residues in the pyrimidine strand are expected to be protonated, assuming the pK_a to be 4.7 (Manzini et al., 1990). Given that the remaining cytosine residues in the third strand need to be protonated in order to form the triplex, and that the ΔH for protonation per mole of cytosine residue is 2.8 kcal (Manzini et al., 1990), the total contribution to the ΔH_{CAL} from these residues would be about 11.2 kcal/mol of triplex. This is about 29% of the total enthalpic change for the third strand binding and illustrates the importance of protonation in the overall stability of this triplex.

Table 3: Triplex Free Energy Changes at 25 °C[a]

triplex third strand	d($G_3T_4G_3$)	d($G_3A_4G_3$)	d($C_3T_4C_3$)
$\Delta G°$(total) (kcal/mol)			
$\Delta G°$	18.4 ± 0.9	22.9 ± 0.1	19.5 ± 0.5
$\Delta G°_{VH(uv)}$	18.8 ± 1[b]		19.2 ± 1[c]
$\Delta G°$(1) (kcal/mol)			
$\Delta G°$	5.6 ± 0.1		6.4 ± 0.1
$\Delta G°_{VH(uv)}$	5.9 ± 0.4[b]	–	6.4 ± 0.5[c]
$\Delta G°$(2) (kcal/mol)			
$\Delta G°$	12.8 ± 0.2		13.1 ± 0.1
$\Delta G°_{VH(uv)}$	12.9 ± 0.6[b]	–	12.8 ± 0.5[c]

[a] **1** and **2** denote the first and second transitions, respectively, and total denotes the sum of both transitions. Uncertainties in $\Delta G°$ represent the standard deviation of values obtained from the range of ΔH_{CAL} values. [b] Scaria et al. (1995) and unpublished data. [c] Pilch et al. (1990a).

The results of Plum et al. (1990) are of particular interest as they observed a very large $\Delta H_{VH(uv)}$ relative to ΔH_{CAL} for the dissociation of the third strand of a pyr∗pur·pyr triplex. A more recent study (Plum & Breslauer, 1995) of an intramolecular pyr∗pur·pyr triplex found both $\Delta H_{VH(uv)}$ and $\Delta H_{VH(cal)}$ to be about twice as large as ΔH_{CAL} for dissociation of the third strand. There is another report, on an intramolecular triplex, in which $\Delta H_{VH(uv)}$ was found to be considerably larger than ΔH_{CAL} (Volker et al., 1993). This discrepancy was only seen at pH = 6.7, and not at pH = 5, where the triplex was more stable. The underlying basis of these unusually large van't Hoff enthalpy values remains to be determined.

As indicated above, we have observed some discrepancies as well between ΔH_{CAL} and $\Delta H_{VH(cal)}$ for the PYR and PUR/PYR triplexes. Our more detailed analysis of the PUR/PYR data suggests that triplex aggregation may explain the observation of a van't Hoff enthalpy change that is greater than the model-free calorimetric enthalpy change. End-to-end association is a likely mechansim for such aggregation and could give rise to a cooperative melting unit that is effectively greater than 10 base triplets. Interestingly, the van't Hoff enthalpy changes determined by analysis of UV melting curves for both of these triplexes are in good agreement with the ΔH_{CAL} values. The fact that the calorimetry data were analyzed by simulating the entire heat capacity curves while the UV data were based on the variation of the melting temperature with oligonucleotide concentration may be important in this distinction.

A comparison of the three triplexes studied here shows that the PUR triplex is most thermally stable, i.e. it melts at the highest temperature, simultaneously with the underlying duplex. This single-transition behavior appears to be characteristic of this class of triplex (Chen, 1991; Pilch et al., 1991; Svinarchuk et al., 1995), in contrast to the other two classes of triplexes, which, depending on cation concentrations, often dissociate in two observable transitions. Because of this behavior, it is not possible to obtain thermodynamic data for dissocation of the third strand from a PUR triplex directly; one must resort to subtraction of the result for the duplex measured separately from those corresponding to complete dissociation of the triplex. However, comparison of ΔH_{CAL} and ΔG values in Tables 2 and 3 for triplex dissociation reveals that the PUR triplex is the most stable in terms of both overall enthalpy and free energy. The greater stability of the PUR triplex may be important from a therapeutic view point, because its formation does not require low-pH conditions. Of course, a limitation in the PUR triplex motif arises from a requirement for some minimum number of guanines in the target duplex. However, Pilch and Breslauer (1994) have reported that ligands such as berenil can induce formation of triplexes composed solely of A∗A·T triplets. Thus, it may be possible to overcome this limitation. The large stabilization of the PUR triplex is mainly enthalpic in origin and might be the consequence of better stacking interactions between the adjacent purine residues in the third strand.

The PUR/PYR triplex has the lowest ΔH and ΔG for overall triplex dissociation among the three classes of triplexes studied. The differences in ΔH for the third strand binding between the PUR and PUR/PYR triplexes are remarkable. Substitution of four As in the third strand by four Ts causes this large destabilization. This could be attributed to the difference in the strand orientation, the difference in the stacking interactions between Ts and As, the presence of purine/pyrimidine steps in the third strand, the presence of adjacent nonisomorphous base triplets, etc. Due to the lack of sufficient thermodynamic data on triplex formation, it is difficult to estimate quantitatively the contributions from each of these effects. This information is extremely important in designing triplex-forming oligonucleotides for therapeutic purposes.

In summary, we have used differential scanning calorimetry to characterize the thermodynamics of triplex formation in three different but related triple helices. The PUR triplex is the most stable, while the PUR/PYR triplex is the least stable. The calorimetrically determined values of ΔH and ΔS corresponding to dissociation of the PUR triplex agree well with those determined by van't Hoff analysis, indicating the validity of the two-state model for this in the short oligonucleotide triplex. The larger van't Hoff enthalpy, in comparison to the calorimetric enthalpy, for dissociation of the third strand of the PUR/PYR triplex appears to be due to triplex association. The large thermodynamic stability of the PUR triplex may be characteristic of the pur∗pur·pyr class of triplexes in general. Should this prove to be true under physiological conditions, purine oligonucleotides may be the most effective at targeting guanine-containing duplex sequences for triple helix formation *in vivo*.

ACKNOWLEDGMENT

It is a pleasure to acknowledge Drs. K. J. Breslauer and L. A. Marky for helpful discussions.

APPENDIX

The biphasic melting of a triple helix, ABC, composed of three strands, A, B, and C, can be modeled by the following simple set of sequential bimolecular reactions:

$$\mathrm{ABC} \overset{K_1}{\rightleftharpoons} \mathrm{A} + \mathrm{BC} \overset{K_2}{\rightleftharpoons} \mathrm{A} + \mathrm{B} + \mathrm{C} \tag{1}$$

If all strands are present at the same concentration, C_t, then at low temperature complete triplex formation leads to a triplex concentration of C_t and the following equations hold at any temperature, reflecting stoichiometry and conservation of mass:

$$C_t = [\mathrm{ABC}] + [\mathrm{BC}] + [\mathrm{B}] \tag{2}$$

$$C_t = [\mathrm{ABC}] + [\mathrm{A}] \tag{3}$$

$$[\mathrm{A}] = [\mathrm{BC}] + [\mathrm{B}] \tag{4}$$

$$[\mathrm{B}] = [\mathrm{C}] \tag{5}$$

Here, the brackets represent molar concentration. By defining the corresponding fractional populations of each species as

$$f_\alpha = \frac{[\alpha]}{C_t} \tag{6}$$

where α represents ABC, AB, A, B, or C, we can recast the above equations as

$$1 = f_{\mathrm{ABC}} + f_{\mathrm{BC}} + f_{\mathrm{B}} \tag{7}$$

$$1 = f_{\mathrm{ABC}} + f_{\mathrm{A}} \tag{8}$$

$$\mathrm{f_A} = \mathrm{f_{BC}} + \mathrm{f_B} \tag{9}$$

$$f_{\mathrm{B}} = f_{\mathrm{C}} \tag{10}$$

The equilibrium constants, K_1 and K_2, for the first and second reactions, respectively, are

$$K_1 = \frac{f_{\mathrm{A}} f_{\mathrm{BC}}}{f_{\mathrm{ABC}}} C_t \quad \text{and} \quad K_2 = \frac{f_{\mathrm{B}} f_{\mathrm{C}}}{f_{\mathrm{BC}}} C_t \tag{11}$$

Using the relations above, the equilibrium constant expressions can be written as a pair of coupled, nonlinear equations for the fractions f_A and f_{BC}:

$$f_{\mathrm{A}} = \frac{K_1}{C_t}\left(\frac{1 - f_{\mathrm{A}}}{f_{\mathrm{BC}}}\right) \tag{12}$$

and

$$f_{\mathrm{BC}} = \frac{C_t}{K_2}(f_{\mathrm{A}} - f_{\mathrm{BC}})^2 \tag{13}$$

Equations 7−10 along with equations 12 and 13 completely describe the set of sequential reactions. Their solution permits determination of the excess enthalpy, H_{xs}, of this

system according to the equation

$$H_{xs} = f_A \Delta H_1 + f_B \Delta H_2 \quad (14)$$

The corresponding excess heat capacity, C_p, is then determined by

$$C_p = \frac{\partial H_{xs}}{\partial T} \quad (15)$$

In solving the above equations, we use the standard representation for the equilibrium constants K_i in terms of the corresponding enthalpy changes ΔH_i:

$$K_i = K_i(T_{mi}) e^{(-\Delta H_i/RT)(1-T/T_{mi})} \quad (16)$$

where T_{mi} is the reference temperatures for the two equilibria. In contrast to the case of a single equilibrium, in the case of sequential bimolecular reactions, the physical significance of the T_{mi} is less apparent since the equilibria are coupled. We thus arbitrarily set the T_{mi} as the temperature at which $K_i = C_t/2$.

We have solved the coupled equations, eqs 12 and 13, numerically for the fractional populations and then determined the heat capacity by numerical differentiation of eq 14, using Mathcad (MathSoft, Inc.), with the assumption that the ΔH_i values are constant. The values of ΔH_i which provided the best fit between simulated and experimental data are reported as $\Delta H_{VH(cal)}$ values for the dissociation of the third strand from the triplex and the dissociation of the resulting duplex.

In the case of the pyr∗pur·pyr and pur∗pur·pyr triplexes, where two of the three strands are identical due to sequence symmetry, the appropriate stoichiometric changes in eqs 1−13 can be readily incorporated. If we represent the triplex dissociation process as

$$A_2B \overset{K_1}{\rightleftharpoons} A + AB \overset{K_2}{\rightleftharpoons} 2A + B \quad (17)$$

then the equation for the excess enthalpy can be written as

$$H_{xs} = (1 - f_{A_2B}) \Delta H_1 + f_B \Delta H_2 \quad (18)$$

where f_{A_2B} and f_B are the fractional populations of triplex and single strand, given by $f_{A_2B} = [A_2B]/C_t$ and $f_B = [B]/C_t$.

It is of interest to note that in eqs 14 and 18 the last term contains only ΔH_2. In addition, the coefficients multiplying ΔH_1 and ΔH_2 are monotonically increasing functions of temperature. Thus, when these curves are deconvoluted, the subtransitions are defined by

$$C_{P,i} = \Delta H_i \frac{\partial f_i}{\partial T} \quad (19)$$

where f_i is f_A or f_B in the case of eq 14 and $1 - f_{A_2B}$ or f_B in the case of eq 18 and each subtransition remains positive everywhere with a single maximum. This behavior is in contrast to that corresponding to the more commonly described set of sequential, unimolecular reactions (Biltonen & Freire, 1978).

In the case of the PUR/PYR triplex, we have not only applied the simulation analysis described above but also implemented a simulation in which the enthalpy change for the first transition governing the fractional populations is a separate parameter from the enthalpy change explicitly appearing in the equation for excess enthalpy. Thus, for the low-temperature transition corresponding to dissociation of the third strand, we use $\Delta H_{VH(cal)}$ in eq 16 and $\Delta H_{CAL(sim)}$ in eq 14.

REFERENCES

Best, G. C., & Dervan, P. B. (1995) *J. Am. Chem. Soc. 117*, 1187−1193.

Biltonen, R. L., & Freire, E. (1978) *CRC Crit. Rev. Biochem. 5*, 85−124.

Brenowitz, M., Senear, D. F., Shea, M. A., & Ackers, G. K. (1986) *Methods Enzymol. 130*, 132−181.

Breslauer, K. J., Frank, R., Blocker, H., & Marky, L. A. (1986) *Proc. Natl. Acad. Sci. U.S.A. 83*, 3746−3750.

Breslauer, K. J., Freire, E., & Straume, M. (1992) *Methods Enzymol. 211*, 533−567.

Chen, F. M. (1991) *Biochemistry 30*, 4472−4479.

Ebbinghaus, S. W., Gee, J. E., Rodu, B., Mayfield, C. A., Sanders, G., & Miller, D. M. (1993) *J. Clin. Invest. 92*, 2433−2439.

Escude, C., Francois, J. C., Sun, J. S., Ott, G., Sprinzl, M., Garestier, T., & Helene, C. (1993) *Nucleic Acids Res. 21*, 5547−5553.

Gluick, T. C., & Draper, D. E. (1994) *J. Mol. Biol. 241*, 246−262.

Greenberg, W. A., & Dervan, P. B. (1995) *J. Am. Chem. Soc. 117*, 5016−5022.

Griswold, B. L., Humoller, F. L., & MacIntyre, A. R. (1951) *Anal. Chem. 23*, 192−194.

Hobbs, C. A., & Yoon, K. (1994) *Antisense Res. Dev. 4*, 1−8.

Hopkins, H. P., Hamilton, D. D., Wilson, W. D., & Zon, G. (1993) *J. Phys. Chem. 97*, 6555−6563.

Keniry, M. A., Strahan, G. D., Owen, E. A., & Shafer, R. H. (1995) *Eur. J. Biochem. 233*, 631−643.

Manzini, G., Xodo, L. E., Gasparotto, D., Quadrifoglio, F., van der Marel, G. A., & van Boom, J. H. (1990) *J. Mol. Biol. 213*, 833−843.

Marky, L. A., Patel, D., & Breslauer, K. J. (1981) *Biochemistry 20*, 1427−1431.

McShan, W. M., Rossen, R. D., Laughter, A. H., Trial, J., Kessler, D. J., Zendegui, J. G., Hogan, M. E., & Orson, F. M. (1992) *J. Biol. Chem. 267*, 5712−5721.

Mergny, J. L., Sun, J. S., Rougee, M., Montenaygarestier, T., Barcelo, F., Chomilier, J., & Helene, C. (1991) *Biochemistry 30*, 9791−9798.

Park, Y. W., & Breslauer, K. J. (1991) *Proc. Natl. Acad. Sci. U.S.A. 88*, 1551−1555.

Pilch, D. S. (1991) Ph.D. Dissertation, University of California, San Francisco, CA.

Pilch, D. S., & Shafer, R. H. (1993) *J. Am. Chem. Soc. 115*, 2565−2571.

Pilch, D. S., & Breslauer, K. J. (1994) *Proc. Natl. Acad. Sci. U.S.A. 91*, 9332−9336.

Pilch, D. S., Brousseau, R., & Shafer, R. H. (1990) *Nucleic Acids Res. 18*, 5743−5750.

Pilch, D. S., Levenson, C., & Shafer, R. H. (1991) *Biochemistry 30*, 6081−6088.

Plum, G. E., & Breslauer, K. J. (1995) *J. Mol. Biol. 248*, 679−695.

Plum, G. E., Park, Y. W., Singleton, S. F., Dervan, P. B., & Breslauer, K. J. (1990) *Proc. Natl. Acad. Sci. U.S.A. 87*, 9436−9440.

Plum, G. E., Grollman, A. P., Johnson, F., & Breslauer, K. J. (1995a) *Biochemistry 34*, 16148−16160.

Plum, G. E., Pilch, D. S., Singleton, S. F., & Breslauer, K. J. (1995b) *Ann. Rev. Biophys. Biomol. Struct. 24*, 319−350.

Postel, E. H., Flint, S. J., Kessler, D. J., & Hogan, M. E. (1991) *Proc. Natl. Acad. Sci. U.S.A. 88*, 8227−8231.

Rougee, M., Faucon, B., Mergny, J. L., Barcelo, F., Giovannangeli, C., Garestier, T., & Helene, C. (1992) *Biochemistry 31*, 9269−9278.

Roy, C. (1994) *Eur. J. Biochem. 220*, 493−503.

Scaggiante, B., Morassutti, C., Tolazzi, G., Michelutti, A., Baccarani, M., & Quadrifoglio, F. (1994) *FEBS Lett. 352*, 380−384.

Scaria, P. V., Shire, S. J., & Shafer, R. H. (1992) *Proc. Natl. Acad. Sci. U.S.A. 89*, 10336−10340.
Scaria, P. V., Will, S., Levenson, C., & Shafer, R. H. (1995) *J. Biol. Chem. 270*, 7295−7303.
Shindo, H., Torigoe, H., & Sarai, A. (1993) *Biochemistry 32*, 8963−8969.
Singleton, S. F., & Dervan, P. B. (1992a) *Biochemistry 31*, 10995−11003.
Singleton, S. F., & Dervan, P. B. (1992b) *J. Am. Chem. Soc. 114*, 6957−6965.
Singleton, S. F., & Dervan, P. B. (1993) *Biochemistry 32*, 13171−13179.
Singleton, S. F., & Dervan, P. B. (1994) *J. Am. Chem. Soc. 116*, 10376−10382.
Strahan, G. D., Shafer, R. H., & Keniry, M. A. (1994) *Nucleic Acids Res. 22*, 5447−5455.
Strobel, S. A., & Dervan, P. B. (1992) *Methods Enzymol. 216*, 309−321.
Strobel, S. A., Doucette-Stamm, L. A., Riba, L., Housman, D. E., & Dervan, P. B. (1991) *Science 254*, 1639−1642.
Sun, J. S., & Helene, C. (1993) *Curr. Opin. Struct. Biol. 3*, 345−356.
Sun, J. S., Mergny, J. L., Lavery, R., Montenay-Garestier, T., & Helene, C. (1991) *J. Biomol. Struct. Dyn. 9*, 411−424.
Svinarchuk, F., Paoletti, J., & Malvy, C. (1995) *J. Biol. Chem.* (in press).
Thuong, N. T., & Helene, C. (1993) *Angew. Chem., Inte. Ed. Engl. 32*, 666−690.
Volker, J., Botes, D. P., Lindsey, G. G., & Klump, H. H. (1993) *J. Mol. Biol. 230*, 1278−1290.
Wilson, W. D., Hopkins, H. P., Mizan, S., Hamilton, D. D., & Zon, G. (1994) *J. Am. Chem. Soc. 116*, 3607−3608.
Xodo, L. E., Manzini, G., & Quadrifoglio, F. (1990) *Nucleic Acids Res. 18*, 3557−3564.
Xodo, L. E., Manzini, G., Quadrifoglio, F., van der Marel, G. A., & van Boom, J. H. (1991) *Nucleic Acids Res. 19*, 5625−5631.
Yang, M., Ghosh, S. S., & Millar, D. P. (1994) *Biochemistry 33*, 15329−15337.

BI960966G